A novel ANG-BSA/BCNU/ICG MNPs integrated for targeting therapy of glioblastoma

Fan Lin
The First Affiliated Hospital of Shenzhen University
Xiao-Li Xiong
The First Affiliated Hospital of Shenzhen University
En-Ming Cui
Jiangmen Central Hospital, Affiliated Jiangmen Hospital of Sun YAT-SEN University
Yi Lei (chiefleiyi@gmail.com)
The First Affiliated Hospital of Shenzhen University

Research Article

Keywords: blood-brain barrier, glioblastoma, albumin nanoparticles, bimodal imaging, targeted therapy

Posted Date: May 17th, 2021

DOI: https://doi.org/10.21203/rs.3.rs-523751/v1

A novel ANG-BSA/BCNU/ICG MNPs integrated for targeting therapy of glioblastoma

Fan Lin,[1] Xiao-Li Xiong,[1]En-Ming Cui,[2,3] And Yi Lei[1,4]
[1]*Department of Radiology, The First Affiliated Hospital of Shenzhen University, Health Science Center, Shenzhen Second People's Hospital, 3002 SunGangXi Road, Shenzhen, 518035, China*
[2]*Department of Radiology, Jiangmen Central Hospital, Affiliated Jiangmen Hospital of Sun YAT-SEN University, 23 Beijie Haibang Street, Jiangmen, 529030, China*
[3]*cem2008@163.com*
[4]*chiefleiyi@gmail.com*

Abstract: Nanomedicine can improve the traditional disease treatment by actively targeting and enhancing the controlled release of drugs in the focus tissue in vivo, moreover the integration of diagnosis and treatment can be achieved by using tracer molecules to indicate the accumulation of nanodrugs in the focus. However， almost all chemotherapeutic drugs and gene drugs failed to effectively treat glioblastoma (GBM) on account of the existence of blood-brain barrier (BBB) which play a role in GBM. So far, the survival rate of patients with GBM has been hardly improved. In the present study, we constructed an integrated nanoprobe based on albumin nanoparticles (NPs) for targeted diagnosis and treatment of GBM. The nanoprobe consists of albumin-coated superparamagnetic iron oxide (SPIO), Carmustine (BCNU) and indocyanine green (ICG) to achieve bimodal imaging and drug delivery. And the surface-coupled Angopep-2 (ANG, TFFYGGSRGKRNNFKTEEY) polypeptide can specifically bind to low density lipoprotein receptor-related protein (LRP), which is overexpressed in BBB and GBM cells.

In the in vitro experiments, we verified that the targeting ability of nanoprobes to GBM cells was significantly better than that of the control group. In addition, in the in vivo experiments, nanoprobes significantly increased the accumulation of brain tumors compared with the control group. Cell killing of GBM cells (U87MG) with ANG-BSA/BCNU/ICG magnetic NPs shows a higher inhibitory effect compared with controls. This novel targeting imaging and drug delivery system provides an efficient strategy for targeted therapy and intraoperative localization of GBM.

Keywords: blood-brain barrier; glioblastoma; albumin nanoparticles; bimodal imaging; targeted therapy

1. INTRODUCTION

Blood-brain barrier (BBB) can not only prevent harmful substances from invading the brain, but also shut out drugs. [1]As the main challenge of chemotherapeutic drug delivery, how to cross the BBB efficiently and safely is the key point of nanomaterials targeted therapy strategy.[2, 3] Glioblastoma (GBM) is one of the most common and invasive brain tumors, and even with the most effective surgical treatment, the median overall survival (OS) of patients with GBM remains less than 15 months. [4, 5]In addition, due to the characteristics of heterogeneity and invasiveness of GBM, it is difficult to completely resect the tumor tissues, thus making GBM be prone to recurrence and failing to be cured. [6]In order to achieve preoperative diagnosis and intraoperative positioning, there is an urgent need for the investigation of a relatively safe neurotumor targeted imaging probes.

Carmustine (BCNU) is a small molecule drug with good lipid solubility, which is widely used in the treatment of glioma due to its excellent permeability across the blood-brain barrier. [7-9]However, a short elimination half-life and poor selectivity increase the frequency of systemic administration and lead to severe adverse reactions, including hepatotoxicity, myrow-suppression, and pulmonary fibrosis. [10]Novel delivery methods bypassing the BBB have been underwent ongoing researches. [11]For instance, polymerically delivered BCNU functions in the treatment of GBM; [12]brain targeted delivery of BCNU by nanoparticles modified with tamoxifen and lactoferrin exerts antiproliferative effects in GBM; [13]targeted delivery of etoposide, BCNU and doxorubicin using nanoparticles to human GBM cells inhibits GBM growth in the brain. [14]

The skeleton used in drug nano-delivery system is mainly composed of two kinds of materials, namely natural polymer and synthetic polymer. [15]As for natural polymers, especially albumin, which have unique physical and chemical properties, they are general protein carriers for drug targeting and improving the pharmacokinetic properties of peptides or protein drugs. [16]Furthermore, albumin is a polymer of amino acids connected by peptide bonds, which is beneficial to the embedding and loading of drugs. [17, 18]The application of albumin in transporting drugs can improve their biodegradability and stability, resulting in the slow release and absorption of tumors and inflammatory tissues. [19, 20]Moreover, many lysine residues promote the chemical coupling and modification of albumin. [21]These above characteristics of albumin suggest that albumin can transport therapeutic drugs and achieve tumor targeting at the same time. [22]Therefore, we prepared BCNU loaded albumin NPs as a drug carrier to enhance its anti-tumor effect in GBM.

As for synthetic polymer, superparamagnetism iron oxide (SPIO) is a widely used and relatively safe magnetic resonance T2 contrast agent, [23, 24]which exerts a short half-life *in vivo*, and is easy to be absorbed by reticuloendothelial cells and cleared by macrophages. [25]Indocyanine green (ICG) is a near infrared dye approved by FDA for clinical use. [26]It can be used for not only near infrared fluorescence imaging, but also converting the absorbed light energy into ROS and heat energy to realize photothermal therapy and photodynamic therapy, respectively.[27, 28] The high tissue penetration depth of near infrared fluorescence imaging and the high resolution of magnetic resonance imaging are of great significance to realize the accurate localization of the tumor before operation and the objective definition of the tumor edge during the operation, consequently, they help to guide the surgical resection of the tumor.[29, 30]

Angiopep-2 (ANG, TFFYGGSRGKRNNFKTEEY) polypeptide can specifically bind to low density lipoprotein receptor-related protein (LRP), which is overexpressed in BBB and GBM cells. [31]Accordingly, in this study, we constructed bovine serum albumin (BSA) NPs (ANG-BSA/BCNU/ICG MNPs) containing SPIO, BCNU and ICG coupled ANG. [31, 32]The *in vitro* and *in vivo* MRI/FL dual mode imaging of GBM were systematically evaluated in order to reflect the penetration ability of BBB and tumor-specific targeting effect. Meanwhile, we evaluated the ability of ANG-BSA/BCNU/ICG MNPs in inhibiting tumor in comparison with control group by conduction of experiments *in vitro* and *in vivo*.[33, 34]

2. MATERIALS AND METHODS

2.1 Materials

Iron (III) acetylacetonate, anhydrous benzyl alcohol, glutaric dyaldehyde, 2-(N-Morpholino) ethanesulfonic acid hydrate(MES), N-(3-dimethylamino-propyl)-N'-ethylcarbodiimide hydrochloride (EDC), N-hydroxysuccinimide (NHS) were purchased from Aladdin Shanghai Reagent (China). BSA

and ICG were acquired from Sigma-Aldrich (USA). Ethanol, chloroform and other solvents were obtained from Sinopharm Chemical Reagent (China). BCNU was purchased from Shanghai Yuanye Bio-Technology (China). ANG peptide (TFFYGGSRGKRNNFKTEEY) was synthesized by Shanghai Qiangyao Bio-Technology (China).

2.2 Synthesis of ANG-BSA/BCNU/ICG MNPs

In brief, 5% (w/v) iron (III) acetylacetonate solution was first prepared with anhydrous benzyl alcohol, thereafter, heated to 110℃ for 1 h by a programmed temperature control equipment, afterwards, heated to reflux temperature and refluxed for 40 h under nitrogen atmosphere. And 40 h later, the aforementioned solution was cooled, while the SPIO NPs were precipitated with acetone, washed thoroughly with acetone and dried.

ANG-BSA/BCNU/ICG MNPs were prepared by a desolvation cross-linking method. Firstly, BSA (50 mg), SPIO NPs (10 mg), and ICG (0.5 mg) were dissolved in 10 mL of deionized water. The pH was adjusted to 9.0 after bath-ultrasonic dispersion. Anhydrous alcohol (50 mL) containing BCNU (0.5 mg) was dropwise added to the solution, followed by stirring at room temperature until a precipitate appeared. Secondly, 25% (w/v) glutaraldehyde (25 μL) solution was added to cross-link the amino groups of BSA, thus forming the nanoparticles, which was performed during stirring at room temperature for 12-24 h. Finally, the mixture was centrifuged at 20,000 rpm/min for 30 min to remove nonencapsulated SPIO NPs, ICG, BCNU and organic solvents, followed by washing 3-5 times with deionized water. The solution was redispersed in 5 mL of MES buffer (0.02M, pH 6.5). BSA/BCNU/ICG MNPs were coupled with ANG peptide using the carbon diamine method. Briefly, 8 μL of EDC solution (10 mg/mL in deionized water) and 10 μL of NHS solution (10 mg/mL in deionized water) were added to 1 mL BSA/BCNU/ICG MNPs solution (10 mg/mL) for activating carboxylic groups. After 25 min incubation, the solution of ANG (0.1 mL, 10 mg/mL) was added to the activated solution and the mixture was incubated for 2 h at room temperature, then transferred to incubation at 4℃ overnight. To remove uncoupled ANG, the mixture was centrifuged at 10,000 rpm/min using ultrafiltration tube (MWCO 30kD) by washing 3 times with deionized water. The supernatant, as the final ANG-BSA/BCNU/ICG MNPs, was collected and redispersed in 5 mL deionized water for further use.

2.3 Characterization of ANG-BSA/BCNU/ICG MNPs

2.3.1 Assessment of morphology by transmission electron microscopy (TEM)

The ANG-BSA/BCNU/ICG MNPs sample was diluted to a suitable concentration and redispersed in a bath-ultrasonic for 5 minutes before dripping onto a copper net with carbon support film, which was prepared for the visualization of sample morphology using a TEM (Hitachi, JEM-2100, Japan).

2.3.2 Dynamic light scattering analysis

The hydrodynamic size and surface Zeta potential of ANG-BSA/BCNU/ICG MNPs were assessed by dynamic light scattering (Malvern, ZS90, UN). The hydrodynamic size and surface Zeta potential, whose assessment was an assistant verification method to evaluate whether ANG was conjugated to the BSA/BCNU/ICG MNPs, were analyzed within 24 h in PBS buffer (0.01 M, pH 7.4) to reflect the stability of the nanoprobes.

2.3.3 Fluorescent spectroscopy analysis

The fluorescence intensity of the nanoprobes was assessed by fluorescence spectrometer to evaluate the near infrared fluorescence imaging performance. The emission peak spectra within 800-900 nm were obtained by setting the excitation at 750 nm wavelength.

2.3.4 Drug encapsulation efficiency, loading content and cumulative drug release

Drug encapsulation efficiency was measured by a HPLC (Waters, Alliance 2695, USA) and detected at 230 nm. Firstly, 0.5 mL of ANG-BSA/BCNU/ICG MNPs was dispersed into 4.5 mL of 0.5% pepsin aqueous solution and digested for 5 h at 37°C. Secondly, the permeation was collected after centrifuging for 10 min at 8,000 rpm using ultrafiltration tube (MWCO 30 kD) and detected at 230 nm by HPLC (Waters). At last, the entrapment efficiency and loading content of BCNU were calculated by the formula as listed: entrapment efficiency (E_e, %)=(1-W_t/W_P)x100%; loading content (LC, %)=M_p/M_tx100%, where W_t and W_P represented the total weight of BCNU used in the fabrication and the weight of BCNU in the permeation, respectively; in addition, M_p and M_t stood for the actual amount of BCNU encapsulated in NPs and total amount of NPs, respectively.

BCNU, which was released from the albumin NPs in PBS with two different pH values (pH 5.5 and 7.4) at 37°C, was evaluated using the dynamic dialysis method. A sample (1 mL) was placed in a dialysis bag (3-5 KD), which was then immersed in a 50 mL centrifuge tube containing 50 mL of PBS, being placed in a horizontal shaking incubator at the temperature of 37°C and shook at the speed of 120 rpm/min. Afterwards, the above 1 mL sample was removed from the centrifuge tube and replaced with 1 mL of fresh buffer at regular time intervals. The BCNU concentration in each sample was quantified by HPLC (Waters) at 230 nm. The cumulative release rate, C_R (%), was calculated with the formula as follows: C_R=[(50Cn+ΣCn−1)]/W0×100%, where Cn and Cn−1 were the corresponding drug concentrations in the released solution at the nth and (n-1)th sampling times, while W0 was total amount of BCNU encapsulated in NPs in dialysis bag, respectively.

2.3.5 Cells viability assay

Human primary GBM cell line U87MG and 293T cells which were purchased from the Cell Bank of Type Culture Collection of Chinese Academy of Sciences (Shanghai, China) were incubated in Dulbecco's modified Eagle's medium (DMEM, Thermo Fisher Scientific, Waltham, MA) containing 10% fetal bovine serum (FBS, Thermo Fisher Scientific) and 100 U/ml penicillin/streptomycin (Invitrogen; Thermo Fisher Scientific) in a humidified incubator with 5% CO_2 at 37°C. As for the detection of cell viability, cells were seeded in 96-well plates (5×10^3 per well) and then incubated with BSA/BCNU/ICG MNPs and ANG-BSA/BCNU/ICG MNPs at different concentrations (0, 50, 100, 150 and 200 ng/mL) for 48 h. The growth inhibition rate of each agent was evaluated by MTT assays. The optical density (OD) was measured using a multifunctional microplate reader (PerkinElmer, MA, USA) at a wavelength of 490 nm. Cell viability was calculated as the following formula: Cell viability (%) = OD of sample/OD of control × 100%.

2.3.6 Targeting performance of ANG-BSA/BCNU/ICG MNPs

When U87MG and 293T cells reached 80% confluences, ANG-BSA/ ICG MNPs and BSA/ ICG MNPs were added into cells for 4 h incubation. After washing with PBS, the harvested cells were stained using

Hoechst Kit. Images were captured using a confocal laser scanning microscope system (Leica, TCS SP8, Germany). For *in vitro* MRI imaging, partial harvested cells were resuspended in 1% agarose. T2 relaxation times were calculated using a T2-multi-echos pulse sequence with TR = 3000 ms, TE = 22–352 ms (16TE), FOV = 100× 120 mm2, data ma-trix = 280 × 216, slice thickness = 5 mm, slice gap = 1 mm.

2.3.7 Animal model

Male adult orthotopic GBM nude mice weighting 18–22 g were purchased from YunQiao Biological Technology Co., Ltd. (Nanjing, China). All animal experiments were approved and conducted according to the principles of the Institutional Animal Care Committee from Shenzhen Second People's Hospital.

2.3.8 *In vivo* fluorescence Imaging

For *in vivo* imaging, orthotopic GBM nude mice were randomly divided into two groups (n = 3), afterwards, ANG-BSA/BCNU/ICG MNPs and BSA/BCNU/ICG MNPs were injected into each mouse of the corresponding group through a lateral tail vein, respectively. Images were acquired before injection and at 0.5, 6, 12, 24 and 48 h after injection, respectively. For optical imaging, an IVIS Imaging Spectrum System (PerkinElmer) was applied with an excitation and emission wavelength at 797 and 835 nm, respectively.

2.3.9 *In vivo* MRI Imaging

As a supplement, in vivo MRI imaging was carried out, combined with fluorescence imaging to prove the targeting performance of ANG-BSA/BCNU/ICG MNPs. Orthotopic GBM nude mice were randomly divided into three groups: PBS； BSA/BCNU/ICG MNPs and ANG-BSA/BCNU/ICG MNPs. The above groups were injected into each mouse through tail vein, and MRI examination was performed 12 h after administration.

2.3.10 Statistical analysis

All *in vitro* experiments were performed in triplicates. Quantitative results were recorded as mean ± standard deviation (SD) of the triplicates or the animal treatment group. One-way analysis of variance (ANOVA) or two-tailed independent t-test was performed to evaluate the differences between different groups. P-value<0.05 represented a statistically significant difference.

3. Results

3.1 Characterization of ANG-BSA/BCNU/ICG MNPs

The morphologies, hydrodynamic size and dispersion of ANG-BSA/BCNU/ICG MNPs were measured by TEM and dynamic light scattering, respectively. As shown in Figure 1A, the ANG-BSA/BCNU/ICG MNPs exhibited a well-defined spherical shape with the size of 85 nm±10 nm, and the average hydrodynamic diameter was 121 nm±4.6 nm (Figure 1B). There were little changes in the hydrodynamic size and surface Zeta potential within 1 week, and the NPs were well dispersed in biological medium

(Figure 1C), which indicated that ANG-BSA/BCNU/ICG MNPs possessed an excellent long-term colloidal stability. In addition, ANG-BSA/BCNU/ICG MNPs showed a limited variation in hydrodynamic size after 3 weeks of storage in PBS buffer at 4°C, indicating an excellent stability in aqueous medium (data were not shown). The measurement by vibrating sample magnetometer showed ANG-BSA/BCNU/ICG MNPs had good magnetic properties, the saturation magnetization reached 16.3emu/g, and the hysteresis curve indicated that the NPs had superparamagnetism (Figure 1D).

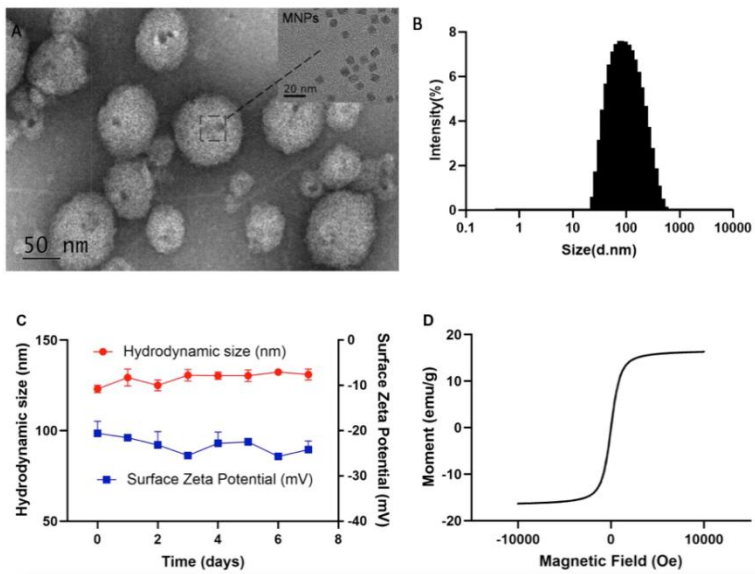

Fig. 1. Characterization of ANG-BSA/BCNU/ICG MNPs presented by transmission electron microscopy and dynamic light scattering. (A) Morphology of ANG-BSA/BCNU/ICG MNPs exerted by transmission electron microscopy. (B) Analysis of hydrodynamic size exhibited by dynamic light scattering. The size ranged from 100 nm to 132 nm. (C) The stability evaluation of ANG-BSA/BCNU/ICG MNPs exhibited by dynamic light scattering. (D) The magnetic properties of ANG-BSA/BCNU/ICG MNPs tested by vibrating sample magnetometer.

3.2 Drug encapsulation efficiency and *in vitro* release

BCNU-loading efficiency was detected by HPLC. The loading content was 30 μg BCNU/mg of Albumin MNPs and the efficiency was about 15%, which showed that ANG-BSA/BCNU/ICG MNPs held an adequate amount of BCNU. Figure 2 demonstrated the release profile of BCNU from ANG-BSA/BCNU/ICG MNPs at pH 7.4 (blood plasma) and pH 5.5 (tumor micro environment), which increased gradually as time went on; especially at 118 h after injection, the release rate was as high as 44.84% and 63.22% at pH 7.4 and pH 5.5, respectively,.

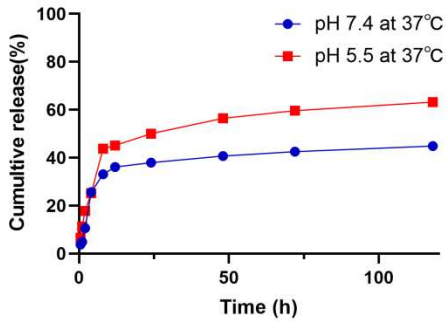

Fig. 2. The *in vitro* release profile of BCNU from ANG-BSA/BCNU/ICG MNPs. The release of BCNU from ANG-BSA/BCNU/ICG MNPs at pH 7.4 and pH 5.5 increased in a time-dependent manner.

3.3 Effect of albumin NPs on cell viability of U87MG and 293T cells

In vitro antitumor activity of BCNU, non-target NPs (BSA/BCNU/ICG MNPs) and target NPs (ANG-BSA/BCNU/ICG MNPs) were assessed in U87MG and 293T cells, respectively. In U87MG cells, no significant difference of cell viability was observed between BCNU and BSA/BCNU/ICG MNPs, while the cell viability was predominantly decreased in ANG-BSA/BCNU/ICG MNPs group in comparison with BSA/BCNU/ICG MNPs group or BCNU group; moreover, the cell viability was reduced by BCNU, BSA/BCNU/ICG MNPs and ANG-BSA/BCNU/ICG MNPs in a dose-dependent manner (Figure 3A). Whereas, in 293T cells, there was no significant difference of cell viability among BCNU, BSA/BCNU/ICG MNPs and ANG-BSA/BCNU/ICG MNPs group; and the cell viability was also reduced by BCNU, BSA/BCNU/ICG MNPs and ANG-BSA/BCNU/ICG MNPs in a dose-dependent manner (Figure 3B).

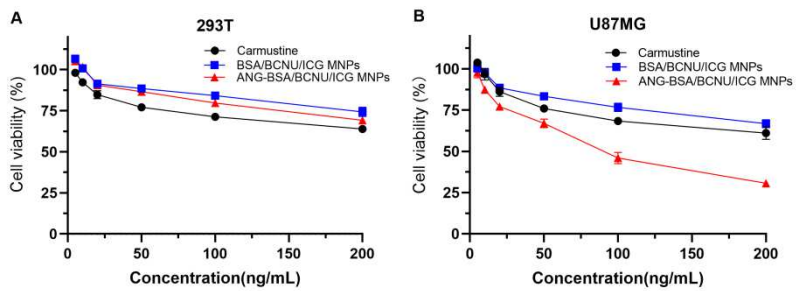

Fig. 3. Effect of albumin NPs on the cell viability of and 293T cells (A) and U87MG cells (B), which was assessed by MTT assays.

As shown in Table 1, there was no significant difference of IC_{50} between BCNU and BSA/BCNU/ICG MNPs in U87MG cells or 293T cells, while there was significantly lower IC_{50} in ANG-BSA/BCNU/ICG MNPs group (one-third at 48 h)when compared with BSA/BCNU/ICG MNPs group or BCNU group in U87MG cellsbut not 293T cells. Taken together, these aforementioned results

demonstrated a higher antitumor activity of ANG-BSA/BCNU/ICG MNPs on GBM compared with BSA/BCNU/ICG MNPs or BCNU.

Table 1. IC_{50} of cells with different treatments by MTT viability assays.

Cell	Treatment	IC_{50} (ng/mL)-48h
293T	Carmustine	412
	BSA/BCNU/ICG MNPs	432 $^{n.s}$
	ANG-BSA/BCNU/ICG MNPs	421 $^{n.s}$
U87MG	Carmustine	301
	BSA/BCNU/ICG MNPs	315 $^{n.s}$
	ANG-BSA/BCNU/ICG MNPs	98$^{\#\#,\ **}$

n.s, no significant difference, BSA/BCNU/ICG MNPs versus BCNU, ANG-BSA/BCNU/ICG MNPs versus BSA/BCNU/ICG MNPs; *## $p < 0.01$* ANG-BSA/BCNU/ICG MNPs versus BCNU，***$p < 0.01$,* ANG-BSA/BCNU/ICG MNPs versus BSA/BCNU/ICG MNPs.

3.4 Targeting performance of ANG-BSA/BCNU/ICG MNPs

The targeting performance of ANG-BSA/BCNU/ICG MNPs was assessed in U87MG cells and 293T cells by using confocal laser scanning microscopy and MRI. In U87MG cells, the red fluorescent signal was stronger in ANG-BSA/BCNU/ICG MNPs group compared with that of BSA/BCNU/ICG MNPs group. However, there was nearly no red fluorescent signal observed in 293T cells which were treated with BSA/BCNU/ICG MNPs or ANG-BSA/BCNU/ICG MNPs (Figure 4). In addition, we incubated different concentrations of NPs with 293T and U87MG cells, then collected the treated cells for MRI detection. And the MRI image showed the similar results with fluorescent signal (Figure 5).

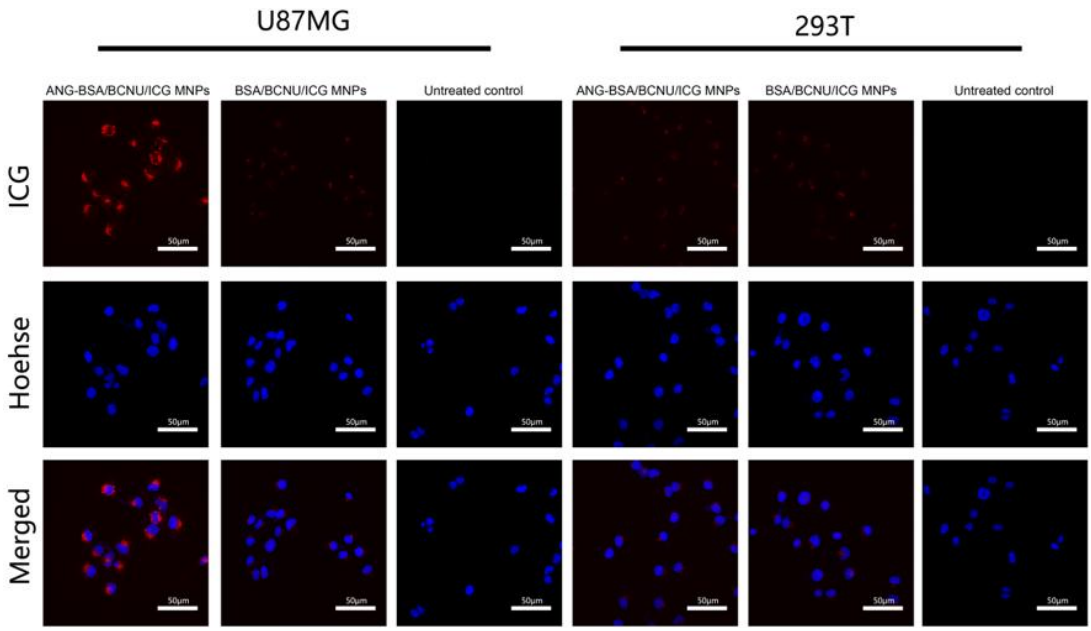

Fig. 4. *In vitro* targeting test of ANG-BSA/BCNU/ICG MNPs by confocal laser microscope (ex/em = 795/835 nm, scale bar = 50 μm)

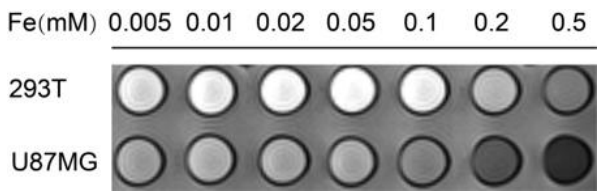

Fig. 5. *In vitro* targeting test of ANG-BSA/BCNU/ICG MNPs by the MRI detection.

3.5 *In vivo* fluorescence Imaging

To further validate BBB penetrating, GBM targeting and the NIRF capabilities of ANG-BSA/BCNU/ICG MNPs, the fluorescence imaging was performed *in vivo*. Take the fluorescence signals at 12 h as an example, they were further presented in BSA/BCNU/ICG MNPs group and ANG-BSA/BCNU/ICG MNPs group, with significantly higher signals in the latter group compared to the former group (Figure 5A). Fluorescence signals of the BSA/BCNU/ICG MNPs group were first detected at 6 h post-injection, then gradually decreased and nearly disappeared at 48 h post-injection; while the fluorescence signals of ANG-BSA/BCNU/ICG MNPs group were first detected at 30 min post-injection, thereafter, peaked at 12 h and remained steady at 48 h post-injection (Figure 5B). In addition, the fluorescence signals of ANG-BSA/BCNU/ICG MNPs group were obviously higher than those of BSA/BCNU/ICG MNPs group at 12 h and 24 h post-injection. These results indicated that ANG-BSA/BCNU/ICG MNPs could obviously cross the BBB and promote NIRF ability.

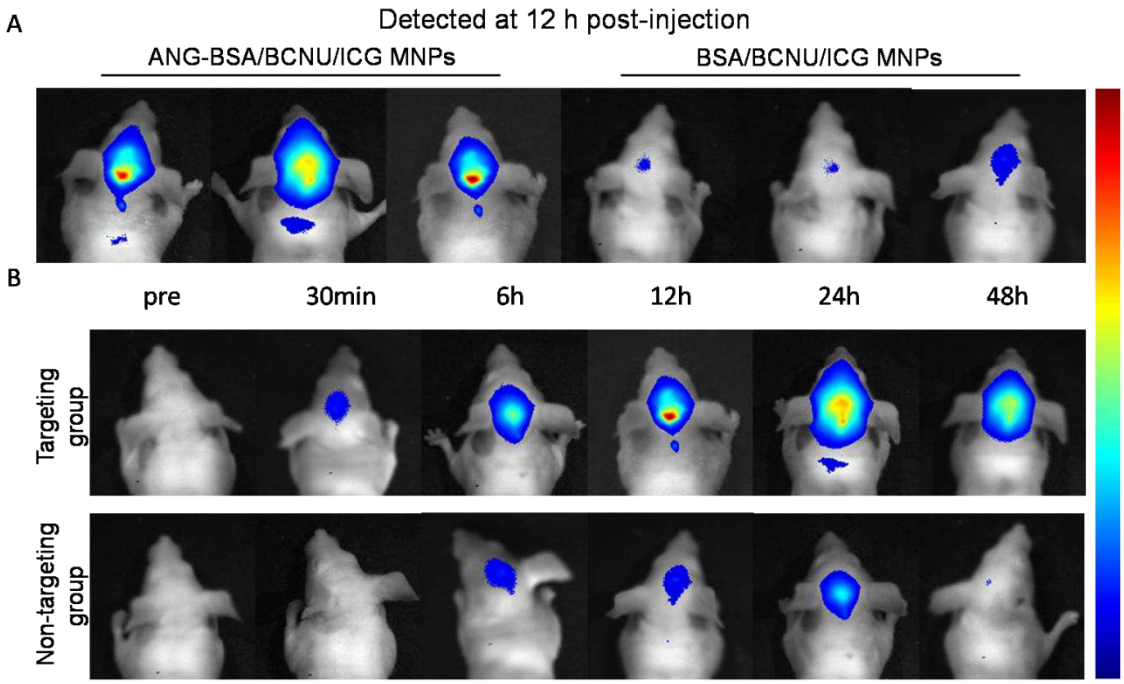

Fig. 6. *In vivo* fluorescence imaging of orthotopic GBM nude mice after intravenously injection of 1.5 mg BCNU-equiv./kg body weight. (A) NIRF images at 12 h post-injection. (B) Head imaging of mice from 0.5 h to 48 h.

3.6 *In vivo* MRI Imaging

Consistent with the results of fluorescence targeting imaging, the ANG-BSA/BCNU/ICG MNPs group showed significant negative enhancement in the brain tumor area, while BSA/BCNU/ICG MNPs showed a relatively small amount of SPIO signals, and these signals did not appear in PBS group. The results showed that ANG-BSA/BCNU/ICGMNPs had a strong targeting imaging ability for glioma, and could clearly display the early size and boundary of the tumor, while loading BCNU did not affect the ability of targeted MRI imaging. It is suggested that ANG-BSA/BCNU/ICGMNPs is helpful for early diagnosis and accurate evaluation of glioma.

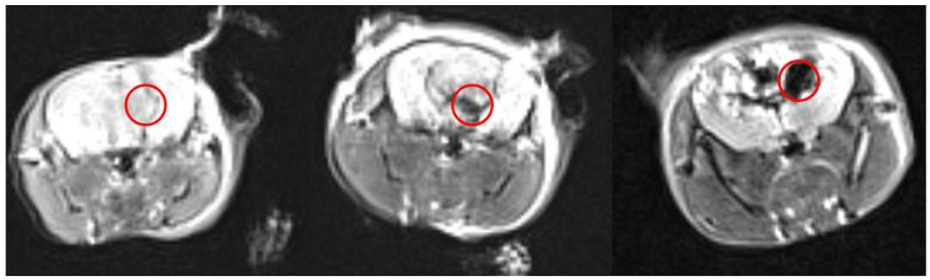

Fig. 7. *In vivo* MRI imaging of orthotopic GBM nude mice after intravenously injection of 11.2 mg SPIO-equiv./kg body weight.

4. Discussion

As acknowledged, the effective treatment of GBM is one of the most difficult challenges in oncology. [6]Despite temozommide (TMZ) combined with radiation is the current contemporary standard of care for GBM, [4]the median OS of patients with GBM is no more than 15 months, which has not been prolonged significantly in the recent 30 years. [5]Therefore, it is of great significance to explore a novel chemotherapeutic drug delivery system with high efficiency and low toxicity for the treatment of GBM.

Nanomedicine can improve the traditional disease treatment by actively targeting and enhancing the controlled release of drugs in the focus tissue in vivo, moreover the integration of diagnosis and treatment can be achieved by using tracer molecules to indicate the accumulation of nanodrugs in the focus. The dual-targeting strategy is expected to accurately transfer drugs or genes to brain tumors, which has shown an advantage over the current tumor or brain targeting strategies and is worthy of further study.

Functionalized albumin NPs, which acts as targeting carrier in this study, had been proved to exhibit numerous advantages, for instance, good biocompatibility, [35]selective toxicity against tumors16, [36]slight side effects [4, 36] and controllable drug release , [37]*etc*. Multifunctional targeting drug delivery system has attracted noticeable attention due to its characteristics of dual therapeutic and diagnostic functions. [38]Accordingly, in the current study, we successfully constructed a multifunctional therapeutic nanoplatform by integrating BCNU, ICG and magnetic nanoparticles, together with angiopep-2 modification for achieving NIRF/MR bimodal imaging and therapy for GBM.

Angiopep-2 has been used as a ligand for brain targeting delivery or dual-targeting to GBM on account of its high binding efficiency to LRP receptor, which is over-expressed in the BBB and GBM cells.[39-41] Consistent with the previous studies, the results from the *in vitro* and *in vivo* fluorescence imaging and MRI imaging had also demonstrated the targeting capability of angiopep-2 in the present work.

Meanwhile, we demonstrated that ANG-BSA/BCNU/ICG MNPs presented good biocompatibility, great colloidal stability, excellent BBB penetration ability and targeting specificity to GBM cells, which were in line with the reports about the functions of albumin NPs in anti-tumor previously. [35-37]We

also indicated that ANG-BSA/BCNU/ICG MNPs exhibited stronger inhibitory effects on GBM cell growth than BSA/BCNU/ICG MNPs or BCNU, which were consistent with the studies about the effects of albumin NPs in inhibiting GBM growth. [42-44]

Collectively, in this study, we developed and characterized a multifunctional ANG-BSA/BCNU/ICG MNPs and tested its properties in both *in vitro* and *in vivo* experimental systems. Taken together, these observations suggest a potential value of ANG-BSA/BCNU/ICG MNPs as a theranostic nanoplatform for targeted therapy and intraoperative localization of GBM.

5. Conclusion

We have successfully developed BBB and GBM targeted and BCNU-loaded NPs. Our results demonstrate its preferential accumulation in tumor sites by NIRF/MRI in a preclinical model. Furthermore, we have demonstrated a superior therapeutic activity of these NPs against GBM. Overall, ANG-BSA/BCNU/ICG MNPs present a promising potential in multifunctional therapy of GBM, and we anticipate that this nanoplatform will be a perfect candidate in GBM theranostic.

Acknowledgements

This study is supported by a grant from Basic Plan Program of
Shenzhen, China (No. JCYJ20180228163333734). We are appreciated for Nanjing Nanoeast Biotech Co., Ltd in rendering the technical support to synthesis of nanoparticles was a gift from Manager Jinxin Li.

Conflict of interests

The authors declare that there was not any type of conflict of interest in the current study.

References

1. S. Agarwal, R. Sane, R. Oberoi, J. R. Ohlfest, and W. F. Elmquist, "Delivery of molecularly targeted therapy to malignant glioma, a disease of the whole brain," Expert Rev Mol Med 13, e17 (2011).
2. Y. Liu, and W. Lu, "Recent advances in brain tumor-targeted nano-drug delivery systems," Expert Opin Drug Deliv 9, 671-686 (2012).
3. S. Osuka, and E. G. Van Meir, "Cancer therapy: Neutrophils traffic in cancer nanodrugs," Nat Nanotechnol 12, 616-618 (2017).
4. P. Y. Wen, and S. Kesari, "Malignant gliomas in adults," N Engl J Med 359, 492-507 (2008).
5. D. Krex, B. Klink, C. Hartmann, A. von Deimling, T. Pietsch, M. Simon, M. Sabel, J. P. Steinbach, O. Heese, G. Reifenberger, M. Weller, and G. Schackert, "Long-term survival with glioblastoma multiforme," Brain 130, 2596-2606 (2007).
6. J. T. Huse, and E. C. Holland, "Targeting brain cancer: advances in the molecular pathology of malignant glioma and medulloblastoma," Nat Rev Cancer 10, 319-331 (2010).
7. X. Xu, X. Chen, X. Xu, T. Lu, X. Wang, L. Yang, and X. Jing, "BCNU-loaded PEG-PLLA ultrafine fibers and their in vitro antitumor activity against Glioma C6 cells," J Control Release 114, 307-316 (2006).

8. G. S. Chae, J. S. Lee, S. H. Kim, K. S. Seo, M. S. Kim, H. B. Lee, and G. Khang, "Enhancement of the stability of BCNU using self-emulsifying drug delivery systems (SEDDS) and in vitro antitumor activity of self-emulsified BCNU-loaded PLGA wafer," Int J Pharm 301, 6-14 (2005).
9. Y. Li, D. H. Ho, B. Tyler, T. Williams, M. Tupper, R. Langer, H. Brem, and M. J. Cima, "In vivo delivery of BCNU from a MEMS device to a tumor model," J Control Release 106, 138-145 (2005).
10. L. D. Rhines, P. Sampath, M. E. Dolan, B. M. Tyler, H. Brem, and J. Weingart, "O6-benzylguanine potentiates the antitumor effect of locally delivered carmustine against an intracranial rat glioma," Cancer Res 60, 6307-6310 (2000).
11. L. D. Rhines, P. Sampath, M. E. Dolan, B. M. Tyler, H. Brem, and J. Weingart, "O6-benzylguanine potentiates the antitumor effect of locally delivered carmustine against an intracranial rat glioma," Cancer Res 60, 6307-6310 (2000).
12. S. D. Wait, R. S. Prabhu, S. H. Burri, T. G. Atkins, and A. L. Asher, "Polymeric drug delivery for the treatment of glioblastoma," Neuro Oncol 17 Suppl 2, i9-i23 (2015).
13. Y. C. Kuo, and S. J. Cheng, "Brain targeted delivery of carmustine using solid lipid nanoparticles modified with tamoxifen and lactoferrin for antitumor proliferation," Int J Pharm 499, 10-19 (2016).
14. Y. C. Kuo, Y. H. Chang, and R. Rajesh, "Targeted delivery of etoposide, carmustine and doxorubicin to human glioblastoma cells using methoxy poly(ethylene glycol)poly(epsiloncaprolactone) nanoparticles conjugated with wheat germ agglutinin and folic acid," Mater Sci Eng C Mater Biol Appl 96, 114-128 (2019).
15. M. Swetha, K. Sahithi, A. Moorthi, N. Srinivasan, K. Ramasamy, and N. Selvamurugan, "Biocomposites containing natural polymers and hydroxyapatite for bone tissue engineering," Int J Biol Macromol 47, 1-4 (2010).
16. F. Kratz, "Albumin as a drug carrier: design of prodrugs, drug conjugates and nanoparticles," J Control Release 132, 171-183 (2008).
17. D. Ni, J. Zhang, W. Bu, H. Xing, F. Han, Q. Xiao, Z. Yao, F. Chen, Q. He, J. Liu, S. Zhang, W. Fan, L. Zhou, W. Peng, and J. Shi, "Dual-targeting upconversion nanoprobes across the blood-brain barrier for magnetic resonance/fluorescence imaging of intracranial glioblastoma," ACS Nano 8, 1231-1242 (2014).
18. R. Yang, Y. An, F. Miao, M. Li, P. Liu, and Q. Tang, "Preparation of folic acid-conjugated, doxorubicin-loaded, magnetic bovine serum albumin nanospheres and their antitumor effects in vitro and in vivo," Int J Nanomedicine 9, 4231-4243 (2014).
19. D. Zhao, X. Zhao, Y. Zu, J. Li, Y. Zhang, R. Jiang, and Z. Zhang, "Preparation, characterization, and in vitro targeted delivery of folate-decorated paclitaxel-loaded bovine serum albumin nanoparticles," Int J Nanomedicine 5, 669-677 (2010).
20. N. Lomis, S. Westfall, L. Farahdel, M. Malhotra, D. Shum-Tim, and S. Prakash, "Human Serum Albumin Nanoparticles for Use in Cancer Drug Delivery: Process Optimization and In Vitro Characterization," Nanomaterials (Basel) 6 (2016).
21. C. Jiang, H. Cheng, A. Yuan, X. Tang, J. Wu, and Y. Hu, "Hydrophobic IR780 encapsulated in biodegradable human serum albumin nanoparticles for photothermal and photodynamic therapy," Acta Biomater 14, 61-69 (2015).
22. X. Song, C. Liang, H. Gong, Q. Chen, C. Wang, and Z. Liu, "Photosensitizer-Conjugated Albumin-Polypyrrole Nanoparticles for Imaging-Guided In Vivo Photodynamic/Photothermal Therapy," Small 11, 3932-3941 (2015).
23. G. Orive, O. A. Ali, E. Anitua, J. L. Pedraz, and D. F. Emerich, "Biomaterial-based technologies for brain anti-cancer therapeutics and imaging," Biochim Biophys Acta 1806, 96-107 (2010).
24. X. H. Li, P. F. Rong, H. K. Jin, W. Wang, and J. T. Tang, "Magnetic fluid hyperthermia induced by radiofrequency capacitive field for the treatment of transplanted subcutaneous tumors in rats," Exp Ther Med 3, 279-284 (2012).

25. Y. Ma, S. Tong, G. Bao, C. Gao, and Z. Dai, "Indocyanine green loaded SPIO nanoparticles with phospholipid-PEG coating for dual-modal imaging and photothermal therapy," Biomaterials 34, 7706-7714 (2013).
26. D. Stanescu-Segall, and T. L. Jackson, "Vital staining with indocyanine green: a review of the clinical and experimental studies relating to safety," Eye (Lond) 23, 504-518 (2009).
27. M. Fadel, N. Samy, M. Nasr, and A. A. Alyoussef, "Topical colloidal indocyanine green-mediated photodynamic therapy for treatment of basal cell carcinoma," Pharm Dev Technol 22, 545-550 (2017).
28. D. Sheng, T. Liu, L. Deng, L. Zhang, X. Li, J. Xu, L. Hao, P. Li, H. Ran, H. Chen, and Z. Wang, "Perfluorooctyl bromide & indocyanine green co-loaded nanoliposomes for enhanced multimodal imaging-guided phototherapy," Biomaterials 165, 1-13 (2018).
29. J. Shi, X. Sun, S. Zheng, J. Li, X. Fu, and H. Zhang, "A new near-infrared persistent luminescence nanoparticle as a multifunctional nanoplatform for multimodal imaging and cancer therapy," Biomaterials 152, 15-23 (2018).
30. L. Deng, X. Cai, D. Sheng, Y. Yang, E. M. Strohm, Z. Wang, H. Ran, D. Wang, Y. Zheng, P. Li, T. Shang, Y. Ling, F. Wang, and Y. Sun, "A Laser-Activated Biocompatible Theranostic Nanoagent for Targeted Multimodal Imaging and Photothermal Therapy," Theranostics 7, 4410-4423 (2017).
31. R. Kurzrock, N. Gabrail, C. Chandhasin, S. Moulder, C. Smith, A. Brenner, K. Sankhala, A. Mita, K. Elian, D. Bouchard, and J. Sarantopoulos, "Safety, pharmacokinetics, and activity of GRN1005, a novel conjugate of angiopep-2, a peptide facilitating brain penetration, and paclitaxel, in patients with advanced solid tumors," Mol Cancer Ther 11, 308-316 (2012).
32. X. Ying, Y. Wang, J. Liang, J. Yue, C. Xu, L. Lu, Z. Xu, J. Gao, Du Y, and Z. Chen, "Angiopep-conjugated electro-responsive hydrogel nanoparticles: therapeutic potential for epilepsy," Angew Chem Int Ed Engl 53, 12436-12440 (2014).
33. M. A. Abakumov, N. V. Nukolova, M. Sokolsky-Papkov, S. A. Shein, T. O. Sandalova, H. M. Vishwasrao, N. F. Grinenko, I. L. Gubsky, A. M. Abakumov, A. V. Kabanov, and V. P. Chekhonin, "VEGF-targeted magnetic nanoparticles for MRI visualization of brain tumor," Nanomedicine-UK 11, 825-833 (2015).
34. M. Zhu, Z. Sheng, Y. Jia, D. Hu, X. Liu, X. Xia, C. Liu, P. Wang, X. Wang, and H. Zheng, "Indocyanine Green-holo-Transferrin Nanoassemblies for Tumor-Targeted Dual-Modal Imaging and Photothermal Therapy of Glioma," ACS Appl Mater Interfaces 9, 39249-39258 (2017).
35. B. Elsadek, and F. Kratz, "Impact of albumin on drug delivery--new applications on the horizon," J Control Release 157, 4-28 (2012).
36. A. O. Elzoghby, W. M. Samy, and N. A. Elgindy, "Albumin-based nanoparticles as potential controlled release drug delivery systems," J Control Release 157, 168-182 (2012).
37. M. Qasim, K. Asghar, G. Dharmapuri, and D. Das, "Investigation of novel superparamagnetic Ni0.5Zn0.5Fe2O4@albumen nanoparticles for controlled delivery of anticancer drug," Nanotechnology 28, 365101 (2017).
38. X. Nan, X. Zhang, Y. Liu, M. Zhou, X. Chen, and X. Zhang, "Dual-Targeted Multifunctional Nanoparticles for Magnetic Resonance Imaging Guided Cancer Diagnosis and Therapy," ACS Appl Mater Interfaces 9, 9986-9995 (2017).
39. S. Huang, J. Li, L. Han, S. Liu, H. Ma, R. Huang, and C. Jiang, "Dual targeting effect of Angiopep-2-modified, DNA-loaded nanoparticles for glioma," Biomaterials 32, 6832-6838 (2011).
40. W. Ke, K. Shao, R. Huang, L. Han, Y. Liu, J. Li, Y. Kuang, L. Ye, J. Lou, and C. Jiang, "Gene delivery targeted to the brain using an Angiopep-conjugated polyethyleneglycol-modified polyamidoamine dendrimer," Biomaterials 30, 6976-6985 (2009).
41. L. Maletinska, E. A. Blakely, K. A. Bjornstad, D. F. Deen, L. J. Knoff, and T. M. Forte, "Human glioblastoma cell lines: levels of low-density lipoprotein receptor and low-density lipoprotein receptor-related protein," Cancer Res 60, 2300-2303 (2000).

42. M. Altunbek, S. Kelestemur, G. Baran, and M. Culha, "Role of modification route for zinc oxide nanoparticles on protein structure and their effects on glioblastoma cells," Int J Biol Macromol 118, 271-278 (2018).
43. C. Li, J. Tan, J. Chang, W. Li, Z. Liu, N. Li, and Y. Ji, "Radioiodine-labeled anti-epidermal growth factor receptor binding bovine serum albumin-polycaprolactone for targeting imaging of glioblastoma," Oncol Rep 38, 2919-2926 (2017).
44. J. H. Mortensen, M. Jeppesen, L. Pilgaard, R. Agger, M. Duroux, V. Zachar, and T. Moos, "Targeted antiepidermal growth factor receptor (cetuximab) immunoliposomes enhance cellular uptake in vitro and exhibit increased accumulation in an intracranial model of glioblastoma multiforme," J Drug Deliv 2013, 209205 (2013).

Figures

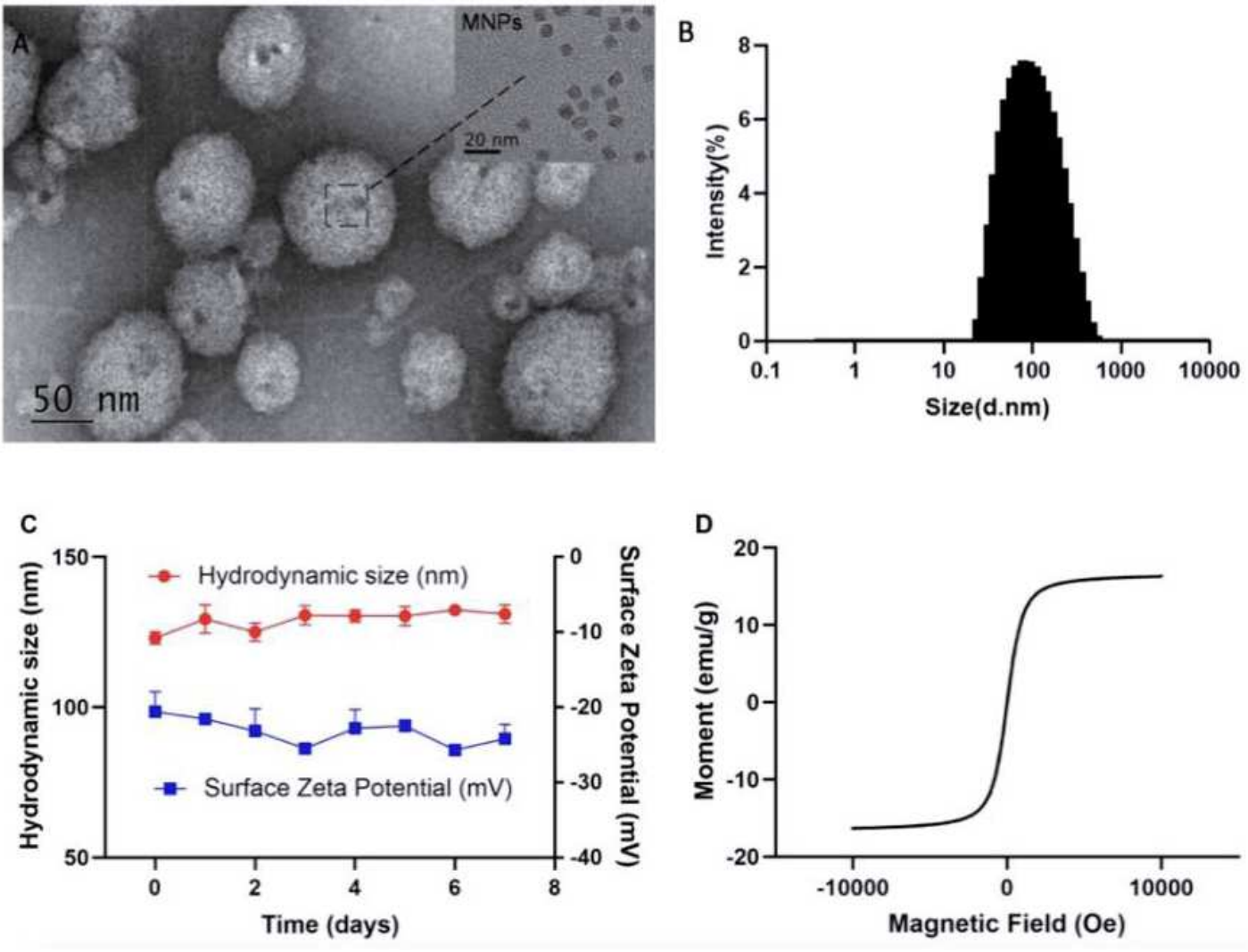

Figure 1

Characterization of ANG-BSA/BCNU/ICG MNPs presented by transmission electron microscopy and dynamic light scattering. (A) Morphology of ANG-BSA/BCNU/ICG MNPs exerted by transmission electron microscopy. (B) Analysis of hydrodynamic size exhibited by dynamic light scattering. The size ranged from 100 nm to 132 nm. (C) The stability evaluation of ANG-BSA/BCNU/ICG MNPs exhibited by dynamic light scattering. (D) The magnetic properties of ANG-BSA/BCNU/ICG MNPs tested by vibrating sample magnetometer.

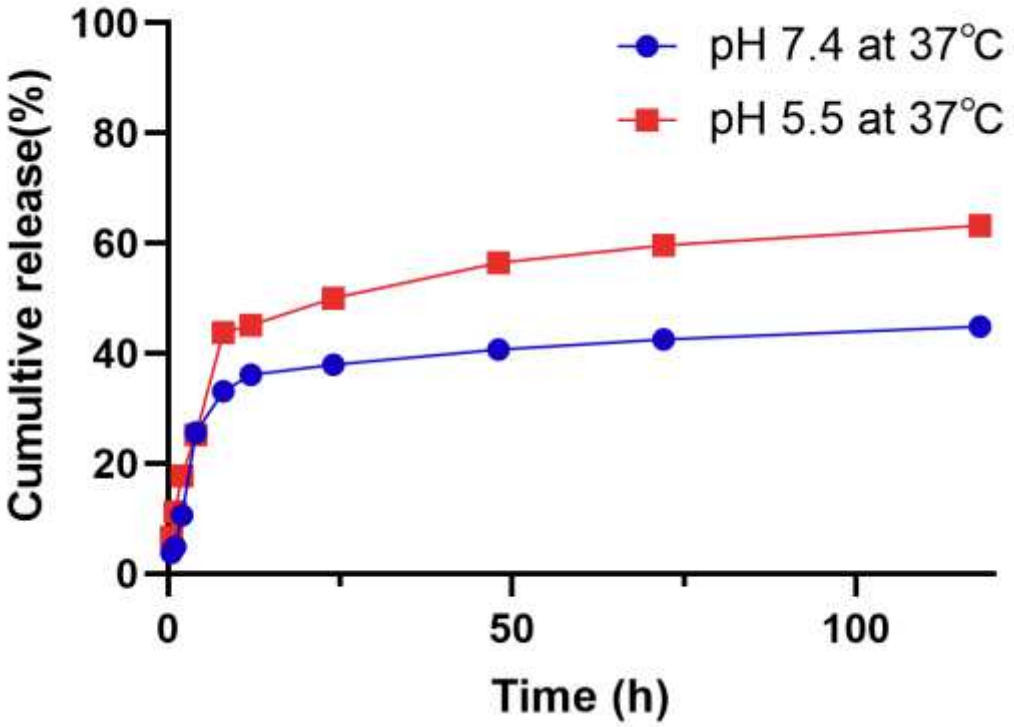

Figure 2

The in vitro release profile of BCNU from ANG-BSA/BCNU/ICG MNPs. The release of BCNU from ANG-BSA/BCNU/ICG MNPs at pH 7.4 and pH 5.5 increased in a time-dependent manner.

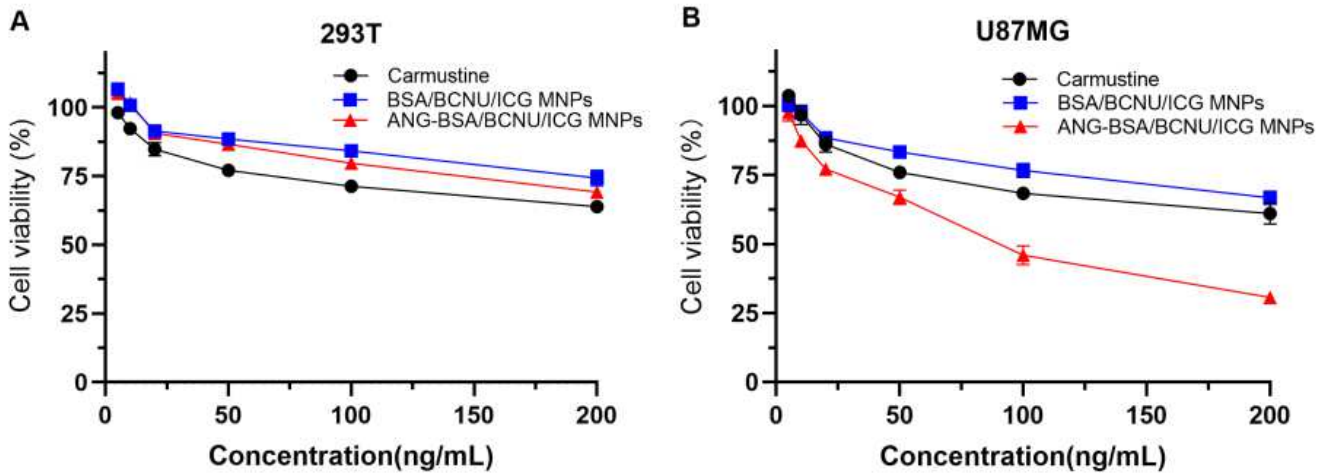

Figure 3

Effect of albumin NPs on the cell viability of and 293T cells (A) and U87MG cells (B), which was assessed by MTT assays.

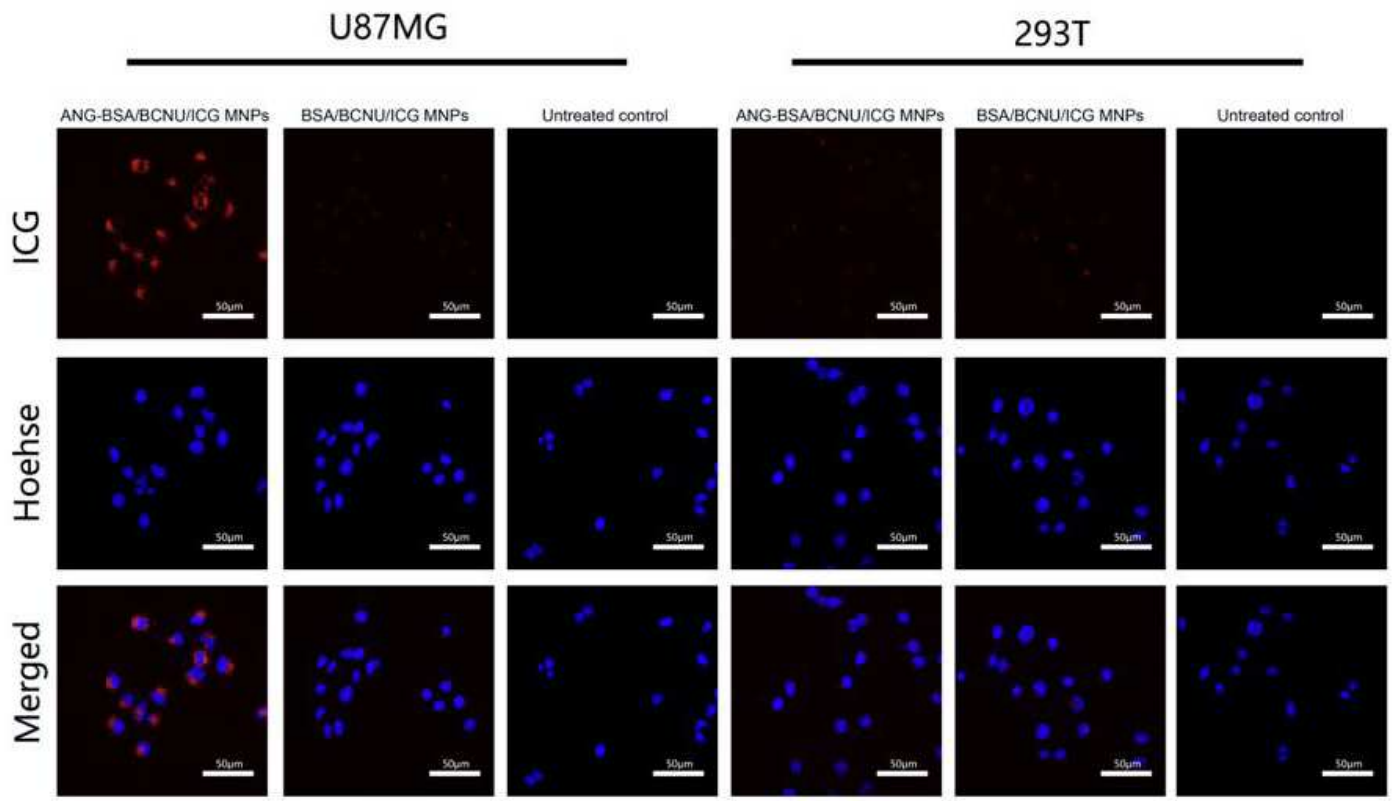

Figure 4

In vitro targeting test of ANG-BSA/BCNU/ICG MNPs by confocal laser microscope (ex/em = 795/835 nm, scale bar = 50 μm)

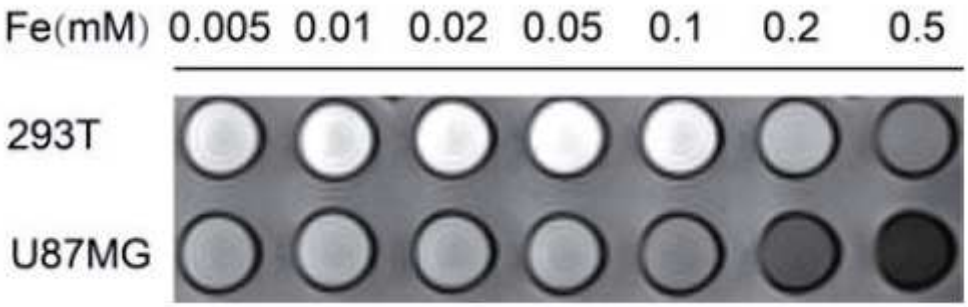

Figure 5

In vitro targeting test of ANG-BSA/BCNU/ICG MNPs by the MRI detection.

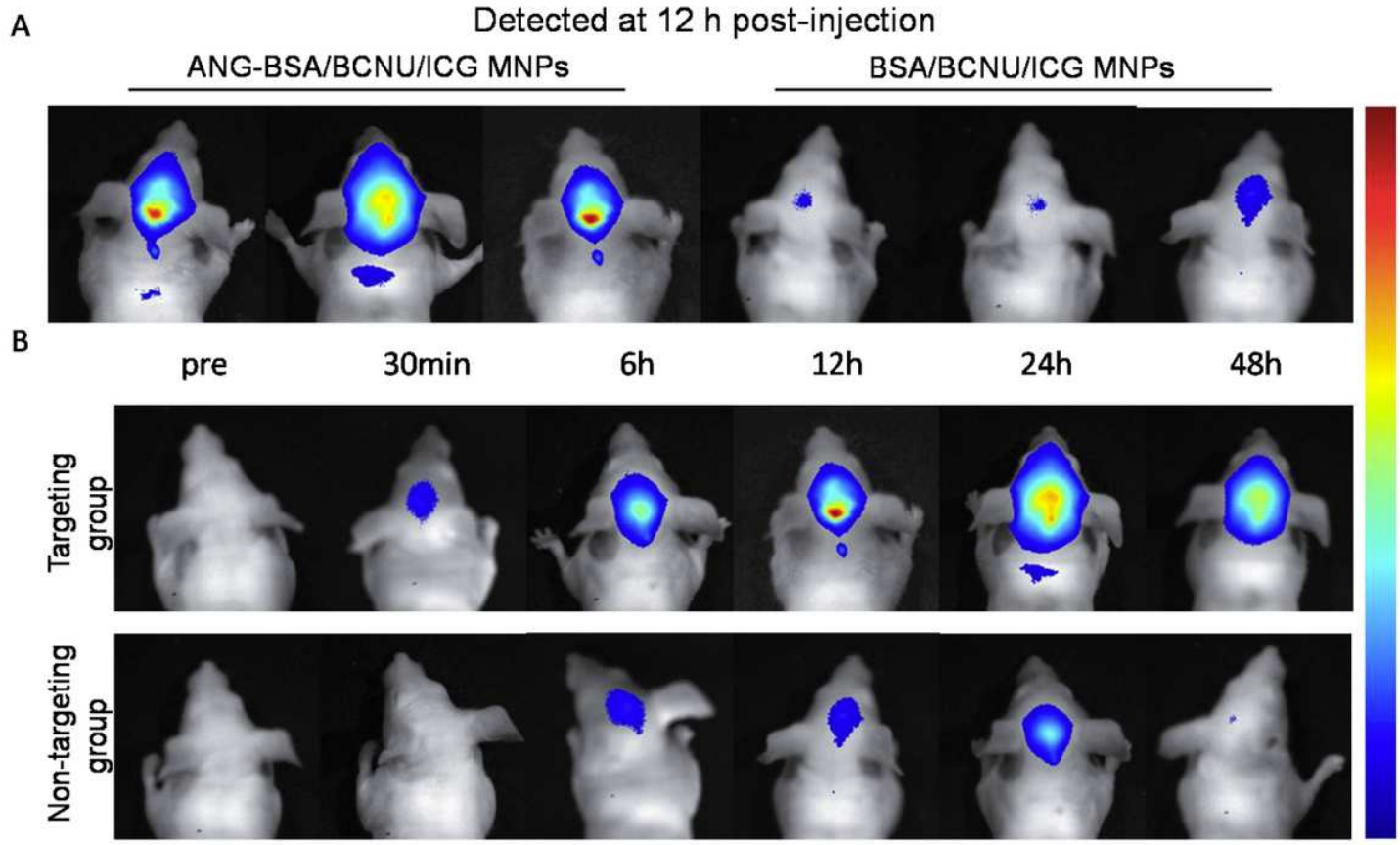

Figure 6

In vivo fluorescence imaging of orthotopic GBM nude mice after intravenously injection of 1.5 mg BCNU-equiv./kg body weight. (A) NIRF images at 12 h post-injection. (B) Head imaging of mice from 0.5 h to 48 h.

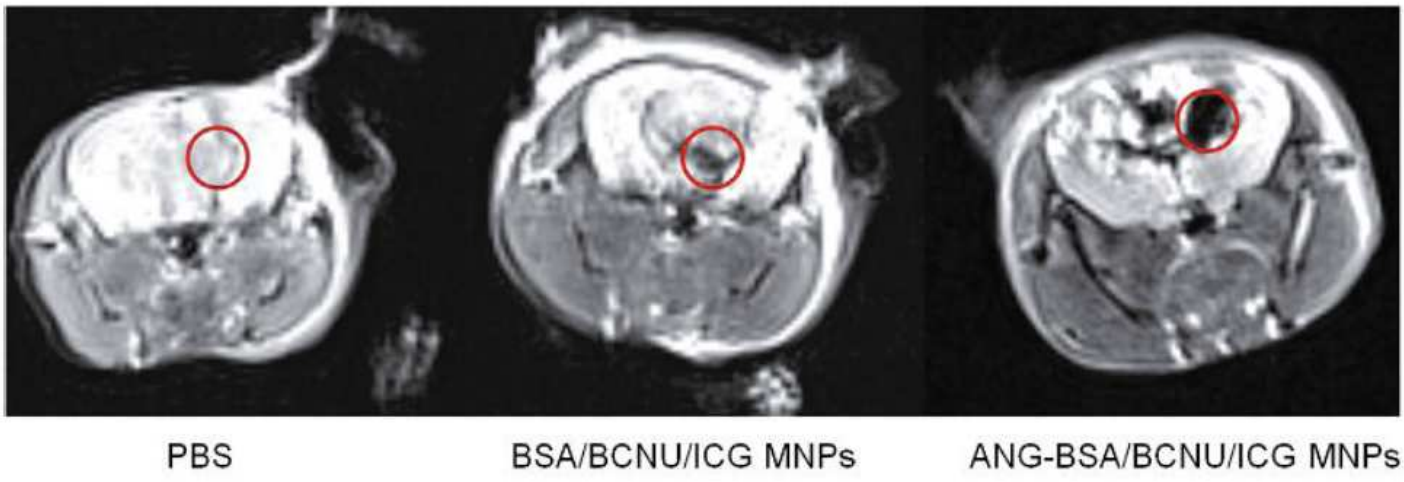

Figure 7

In vivo MRI imaging of orthotopic GBM nude mice after intravenously injection of 11.2 mg SPIO-equiv./kg body weight.